NANO · MICRO small
www.small-journal.com

Self-Assembly Pathways of Triblock Janus Particles into 3D Open Lattices

Hossein Eslami and Florian Müller-Plathe*

The self-assembly of triblock Janus particles is simulated from a fluid to 3D open lattices: pyrochlore, perovskite, and diamond. The coarse-grained model explicitly takes into account the chemical details of the Janus particles (attractive patches at the poles and repulsion around the equator) and it contains explicit solvent particles. Hydrodynamic interactions are accounted for by dissipative particle dynamics. The relative stability of the crystals depends on the patch width. Narrow, intermediate, and wide patches stabilize the pyrochlore-, the perovskite-, and the diamond-lattice, respectively. The nucleation of all three lattices follows a two-step mechanism: the particles first agglomerate into a compact and disordered liquid cluster, which does not crystallize until it has grown to a threshold size. Second, the particles reorient inside this cluster to form crystalline nuclei. The free-energy barriers for the nucleation of pyrochlore and perovskite are ≈10 k_BT, which are close to the nucleation barriers of previously studied 2D kagome lattices. The barrier height for the nucleation of diamond, however, is much larger (>20 k_BT), as the symmetry of the triblock Janus particles is not perfect for a diamond structure. The large barrier is associated with the reorientation of particles, i.e., the second step of the nucleation mechanism.

1. Introduction

The surfaces of colloidal particles can be decorated, thus introducing anisotropic interactions between them. Such colloidal particles with orientation-dependent interactions (patchy particles, Janus particles) are of special interest. Compared to isotropic particles, they allow a wider variety of self-assembled structures. Tuning the number of patches and the magnitude of patch-patch interactions has opened up a bottom-up approach for fabrication of a number of interesting supracolloidal structures, such as Janus clusters,[1–3] chains,[4] Janus cylinders,[5] and 2D lattices[6] via self-assembly. The directional bonding and the feasibility of controlling the patch-patch interactions[7] offers a possibility of assembling Janus colloidal particles to low-coordination structures, making them ideal candidates for the fabrication of two- and 3D photonic band gap materials.[8,9] Because of their ability to control propagation of light, such materials have found diverse applications including optical fibers, sensors, and optoelectronic devices.[10]

Among patchy colloidal particles, the triblock colloidal particles, which are simple to synthesize,[2,6] have emerged as a new class of building blocks for the fabrication of colloidal open crystals. Therefore, the application potential of triblock Janus particles for the manufacture of optical materials with photonic band gaps has attracted a great deal of interest.[10] Although there has been a significant advancement in the self-assembly of tailored Janus particles, the resulting structures have been limited to 2D open and close packed structures[6] and to 3D unstructured clusters[2,3] of Janus particles. As yet, there is no report on the assembly of regular 3D lattices from colloidal Janus building blocks. It is worth mentioning that in the last two decades, with taking advantage of programmable recognition and hybridization interactions between DNA strands,[11,12] the DNA coated colloidal particles have been shown to form bridges with complementary DNA strands to promote self-assembly to face-centered cubic (fcc) and body-centered cubic (bcc) crystal structures.[13] Only recently, this technique has been extended to the self-assembly of more challenging lattices like diamond.[14]

In addition to the synthetic challenges to fabricate anisotropic particles, a major challenge is to exploit available and potential patchy particles to self-organize into desired ordered structures, which can form advanced functional materials and devices. In this respect, a fundamental understanding of the relation between the architecture of the particles and the properties of the resulting assemblies plays an important role.[15] Computer simulation has a leading role in the exploration of mechanism of nucleation and phase transitions. It is easy to design particles with multiple well-ordered patches and to tune their interactions. Computer simulations have been used to study many processes in patchy-particle systems, including self-assembly, pathway to nucleation, and crystallization.[16–19] In the first modeling

H. Eslami
Department of Chemistry
College of Sciences
Persian Gulf University
Boushehr 75168, Iran
E-mail: h.eslami@theo.chemie.tu-darmstadt.de
H. Eslami, F. Müller-Plathe
Eduard-Zintl-Institut für Anorganische und Physikalische Chemie
Technische Universität Darmstadt
Peter-Grünberg-Straße 8, 64287 Darmstadt, Germany

The ORCID identification number(s) for the author(s) of this article can be found under https://doi.org/10.1002/smll.202306337

DOI: 10.1002/smll.202306337

schemes, the Janus particles were treated as hard-spheres, plus angle-dependent square-well terms to address the patch-patch interactions, that is, the Kern–Frenkel potential.[20] In subsequent simulation studies, the models have been taken forward to include softness in the Janus particle potential,[21–26] which is shown to promote self-assembly of open lattices.[27,28]

Molecular simulation studies on the self-assembly of 3D open lattices consist of designing patchy particles with a desired number of patches at appropriate locations on the surface.[23,29–32] For example, Janus particles consisting of four tetrahedrally arranged patches have been employed as building blocks for the self-assembly of a diamond lattice,[23,29–31] using the Kern-Frenkel[20] or similar single site potentials plus directional attractive interactions. These models typically use an implicit solvent. Because of the ease of synthesizing two-patch (triblock) Janus particles, compared to more than two patch particles at desired geometries, more attention has been paid in the recent simulation studies to their self-assembly into open 3D lattices,[33] for which no experimental reports exist. Using a single site repulsive core model, modulated by orientation-dependent attractions, a two-stage process has been designed to self-assemble the perovskite, pyrochlore, and diamond lattices.[34–37] In the first stage, stable tetrahedral and octahedral clusters were formed from triblock Janus particles. To avoid polydispersity, the second stage has been limited to the self-assembly of primary tetrahedral and octahedral building blocks into pyrochlore/diamond and perovskite lattices, respectively. The authors reported that because of the initial formation of clusters of different sizes, a single stage assembly, by which such open lattices would directly self-assemble from a solution of individual triblock Janus particles as building blocks, had not been possible.[34–37] Using the Kern–Frenkel model,[20] recently Rivera-Rivera et al.[38] have inverse designed triblock Janus particles which self-assemble to the pyrochlore lattice.

Very recently, we have developed detailed dissipative particle dynamics[39] (DPD) models of triblock Janus particles with explicit attractive patches and surface charges on the particles.[40–42] We have also included an explicit solvent (water) in the model. It has been shown[40–42] that the use of this detailed model allows elucidation of the role of the surface chemistry, solvent, and hydrodynamic interaction on the self-assembly mechanism, and that compared to simplified models, results closer to experiment are obtained. It is worth mentioning that hydrodynamic interactions are shown to enhance self-assembly of colloidal particles.[43] In this work we report simulation results by this detailed model on the self-assembly of triblock Janus particles into 3D open lattices. We go beyond the existing literature by also allowing a single-stage self-assembly, i.e., the building blocks are the triblock Janus particles themselves, not preformed clusters of them. We report the structural evolution of the solution of Janus particles in water and the types of 3D lattices self-assembled from them, depending on the size of the hydrophobic patches, as well as the mechanism of their self-assembly. Furthermore, we calculate the free energy barriers to nucleation of each lattice and we investigate the dynamics of self-assembly.

2. Method

Self-assembly of colloidal particles to ordered structures normally involves surmounting high free energy barriers, which are unlikely to be overcome within the time scales of brute-force molecular-dynamics simulations.[44] Advanced sampling schemes have been proposed to sample the configuration space along a number of order parameters, used to identify the reaction path.[45] In this work, we have employed our previously developed adaptive-numerical-bias metadynamics[46] scheme to fill the free energy basins with adaptive biasing potentials. Accumulating the probability density along an order parameter, q, the Gibbs free energy, G, can be calculated as:

$$G\ (q) = -k_B T \ln\left(P\left(q\right)\right) \tag{1}$$

where k_B is the Boltzmann constant, T is the temperature, and $P(q)$ is the probability of observing q between q and $q + dq$.

In the adaptive-numerical-bias metadynamics, history-dependent biasing potentials, based on the accumulated statistics of the order parameter during a time interval δt, are added to the unbiased potential energy of the system.

$$\Delta U\ (q,t) = -k_B T \sum_{t'} \ln\left(P\left(q\left(t'\right)\right)\right) \tag{2}$$

where t is time, $t - \delta t < t' \leq t$, and $\Delta U(q, t)$ is the biasing potential. It has been shown that the sum of history-dependent numerical biasing potentials converges to $\Delta G(q)$.[46]

To drive simulations from one phase to another one, proper order parameters must be chosen that distinguish between different phases. Historically, Steinhardt bond order parameters[47] have been used to measure the local order around a particle. The local order, $q_{lm}(i)$, around a particle i is defined as:

$$q_{lm}\ (i) = \frac{1}{N_b\ (i)} \sum_{j \in N_b(i)} Y_l^m\left(\theta_{ij}, \varphi_{ij}\right) \tag{3}$$

where θ_{ij} and φ_{ij} are the azimuthal and polar angles, specifying the orientation of a bond connecting particle i to a neighboring particle j, Y_l^m are the spherical harmonics, and $N_b(i)$ is the number of neighbours of particle i, within a cutoff distance. Based on the dot products proposed by van Duijneveldt and Frenkel,[48] we have presented the following two local order parameters for distinguishing liquid and different crystalline phases.[49]

$$q_l\ (i) = \mathbf{q_l}\ (i) \cdot \mathbf{q_l}\ (j) = \frac{1}{N_b\ (i)} \sum_{j \in N_b(i)} \sum_{m\ =\ -l}^{l} \hat{q}_{lm}\ (i)\, \hat{q}_{lm}^{*}\ (j) \tag{4}$$

where

$$\hat{q}_{lm}\ (i) = \frac{q_{lm}\ (i)}{\left(\sum_{m=-l}^{l} \left|q_{lm}\ (i)\right|^2\right)^{1/2}} \tag{5}$$

The neighbor-averaged local order parameters are defined as:[49]

$$\bar{q}_l\ (i) = \frac{1}{N_b\ (i) + 1}\left(q_l\ (i) + \sum_{j \in N_b(i)} q_l\ (j)\right) \tag{6}$$

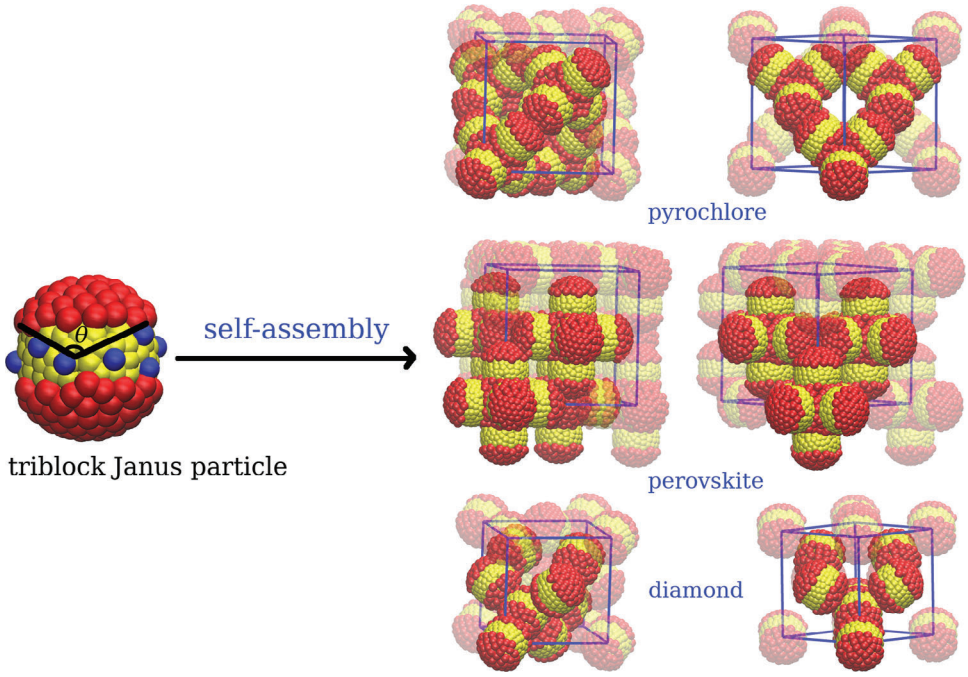

Figure 1. (left) A triblock Janus particle with patches of the same width, θ, on the poles. The blue spheres in the equatorial region represent the surface charges. (right) Schematic representation of open crystal structures assembled from triblock Janus particles. Representative views of the conventional unit cells as well as the motifs, depicted as more colorful particles, for each lattice are shown. For pyrochlore, the unit cell consists of 16 particles, i.e., the four corner-sharing tetrahedra. Four corner-sharing octahedra construct the unit cell of perovskite lattice. The unit cell of diamond consists of eight Janus particles. The tetrahedral subunits in diamond consist of five Janus particles.

In this work, the local order parameters $\bar{q}_l(i)$ are chosen to drive simulations for sampling the configuration space in our biased simulations.

3. Model and Simulation Details

We consider our detailed model[40–42] of triblock Janus particles developed previously to represent experimentally synthesized[2,6] colloidal particles. The experimental triblock Janus particles, employed as building blocks for the self-assembly of 2D kagome and hexagonal phases on a substrate, are made of polystyrene (PS) sulfonate. Their equatorial region is charged, and hydrophobic *n*-octadecanethiol patches decorate their poles. The Coulombic repulsion between the equatorial regions can be tuned by addition of salt to the solution, thereby decreasing the Debye screening length. The particles self-assemble, through the balanced attractive (patch-patch) and repulsive interactions, to a 2D kagome lattice[6] and to 3D clusters.[2,6]

To provide a computationally affordable model, we have proposed[40–42] many-body dissipative particle dynamics[50] (DPD) model of the triblock Janus particles, solvent, and hydrated cations. In many-body DPD, an attractive force is added to the conservative force, $\mathbf{F}_{ij}^{C}$, of the conventiaonl DPD, i.e.,

$$\mathbf{F}_{ij}^{C} = \begin{cases} \left[A_{ij}\left(1-\frac{r_{ij}}{r_C}\right) + B\left(\bar{\rho}_i+\bar{\rho}_j\right)\left(1-\frac{r_{ij}}{\lambda r_C}\right)\right]\hat{\mathbf{r}}_{ij} & r_{ij} \le \lambda r_C \\ A_{ij}\left(1-\frac{r_{ij}}{r_C}\right)\hat{\mathbf{r}}_{ij} & \lambda r_C \le r_{ij} \le r_C \\ 0 & r_{ij} > r_C \end{cases} \quad (7)$$

where $A_{ij}(A_{ij} < 0)$ and $B(B > 0)$ are the strengths of attractive and repulsive forces, respectively, r_{ij} is the distance between beads i and j, respectively, r_C is the cutoff distance, λ is a constant ($\lambda < 1$), $\mathbf{r}_{ij} = \mathbf{r}_{ij}/r_{ij}$, and $\bar{\rho}_i$ and $\bar{\rho}_j$ are the average local densities around beads i and j, respectively. A combination of random and dissipative forces constructs the DPD thermostat.

The DPD beads for solvent (water) and cations each consists of five water molecules and single cations hydrated with five water molecules, respectively. The spherical core (diameter 5.50 nm) of the particle is a highly cross-linked PS chain of 330 monomers. The monomers, each represented by a single DPD bead, are connected through harmonic springs. The equilibrium bond length (0.55 nm) corresponds to the monomer-monomer bond length in coarse-grained models of PS.[51] A structural anchor consisting of three beads in a linear configuration, cocenter with the core sphere, is employed to keep the surface beads unambiguously in each hemisphere. The surface beads in each hemisphere are grafted to their neighboring beads and to the anchor beads. Single DPD beads, forming the hydrophobic patches, are grafted to all surface beads at the poles. About 10% of the equally spaced equatorial beads of the nanoparticle are grafted with the hydrated sulfonate anions, each represented as one DPD bead. Therefore, the number of sulfonate beads depends on the patch width. A configuration of a triblock Janus particle is shown in **Figure 1**. The opening angle, θ, in Figure 1 defines the patch width.

A ≈30 wt.% solution of triblock Janus particles in water, in which the particles were randomly distributed in the solvent, was prepared for performing nucleation/crystallization simulations. All many-body DPD[50] simulations were done with

our simulation package, YASP.[52] The electrostatic interactions were calculated using our previously developed Gaussian charge distribution method.[53] The time step for integration of equations of motion was 0.1 ps. Starting from an initial configuration, which Janus particles were distributed randomly in the simulation box, simulations were done in the constant pressure-constant temperature (NpT) ensemble. The NpT-ensemble simulations were continued to a state at which a large enough cluster (around 50 particles) was formed. Subsequently, metadynamics simulations, up to 5.8 µs long, were done. Two set of metadynamics simulations were performed. In one set, the local-order-parameters $\bar{q}_6$ and $\bar{q}_4$ were chosen as the driving coordinates to find the phase boundaries, depending on the patch width, and to calculate the melting points of the involved lattices. In another set, to investigate the mechanism of nucleation, metadynamics simulations in the space of the cluster size (see bellow) and the crystal size were done. The statistics of the order parameters was accumulated over a time widow $\delta t = 10$ ps for the calculation of the adaptive biasing potentials. The maximum height of the deposited biasing potentials was $0.5k_BT$.

4. Results and Discussions

4.1. Distribution of Local Order Parameters

To drive simulations between liquid and candidate crystalline structures, the choice of proper order parameters, discriminating between different structures, is a determining factor. Provided that the chosen order parameters (in this work $\bar{q}_6$, $\bar{q}_4$) could not differentiate the phases involved, more sensitive order parameters should be employed to be able to drive the simulations between them. Normally, depending on the choice of l in Equation 6, one can tune the sensitivity of the order parameter to the local environment.

We have done simulations on the liquid and on the candidate open crystalline phases of triblock Janus particles. Our test simulations showed that three (open) solid structures can possibly exist: pyrochlore, perovskite, and diamond, whose structures are shown in Figure 1.

To examine the ability of the proposed order parameters to distinguish different phases, we did simulations at temperatures 10% below the melting points of the lattices, as calculated from metadynamics simulations. The distributions of local order parameters ($\bar{q}_6$, $\bar{q}_4$) for the liquid, pyrochlore, perovskite, and diamond phases are shown in **Figure 2**. The distributions for all phases are distinguishable when both these two order parameters are selected. Thus, the different phases involved in the biased sampling simulations can be discriminated.

4.2. Nucleation of Pyrochlore, Perovskite, and Diamond from Solution

We have done biased sampling simulations on Janus particles with patch widths range $50° < \theta < 145°$ at 10° intervals to investigate the effect of patch width on the stabilities of the candidate structures. Finer resolution simulations were done close to phase boundaries to find their exact locations. The two order parameters $\bar{q}_6$ and $\bar{q}_4$, Equation 6, were employed to drive simulations

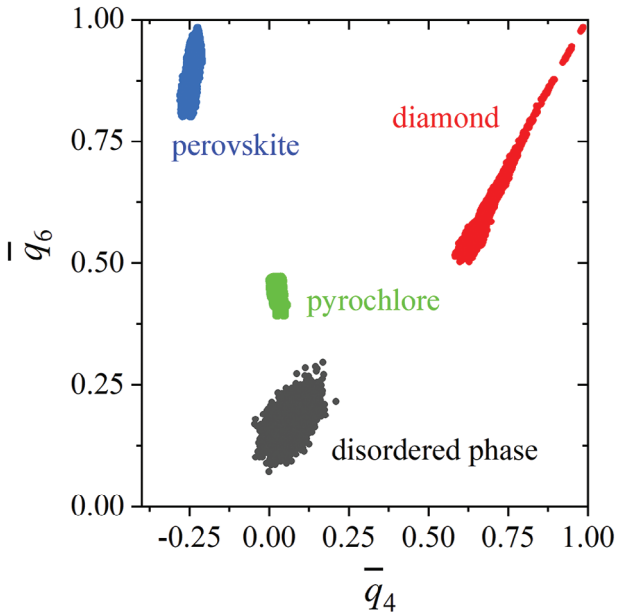

Figure 2. Distributions of the local order parameters ($\bar{q}_6$, $\bar{q}_4$) for liquid, pyrochlore, perovskite, and diamond phases. For solid phases the distributions are obtained from simulations at temperatures 10% below their respective melting temperatures.

from the liquid to the crystalline phases and back. Our previous biased-[40,41] and unbiased-[28,42] simulations on the self-assembly of triblock Janus particles reveal that the bias does not influence the mechanism of self-assembly and the stabilities of involved phases.

Our results show that pyrochlore is the stable phase for patch widths $56° < \theta < 87°$. To form a pyrochlore lattice, the four Janus particles making the tetrahedral subunits should attach together at the center of a tetrahedron (see Figure 1). Over the width range $56° < \theta < 87°$, the patches are wide enough to allow three contacts per patch, required to stabilize such tetrahedral subunits and, hence, the pyrochlore lattice. Previous experimental[6] and simulation[16,22,28,40–42] reports reveal that a patch of size $\theta \geq 60°$ forms two bonds in a 2D packing and thus, stabilizes a 2D kagome lattice. Expectedly, such a patch width allows for three bonds in three dimensions. For perovskite, the octahedral motifs (Figure 1), establish four contacts per patch. Wider patches, $87° < \theta < 122°$, allow four contacts per patch and stabilize the perovskite lattice, which is denser than pyrochlore. Among the three candidate lattices, diamond has the lowest density. Four narrow patches per particle, pointing to the corners of a tetrahedron, would have the perfect symmetry for building a diamond lattice. In the present triblock Janus particles, with two patches at the poles, diamond can potentially self-assemble, provided that each patch is wide enough, $\theta > 109°$, to cover the whole area between the two patches in tetrahedrally patched particles. If θ is close to 109°, however, only the patch edges contact in tetrahedral subunits of diamond. In this geometry, the contact area between patches of different particles is too small to form stable bonds. Therefore, wider patches are needed to stabilize the diamond lattice. Our simulations show that patches ($125° < \theta < 135°$) wide enough to allow a tetragonal arrangement of five particles with

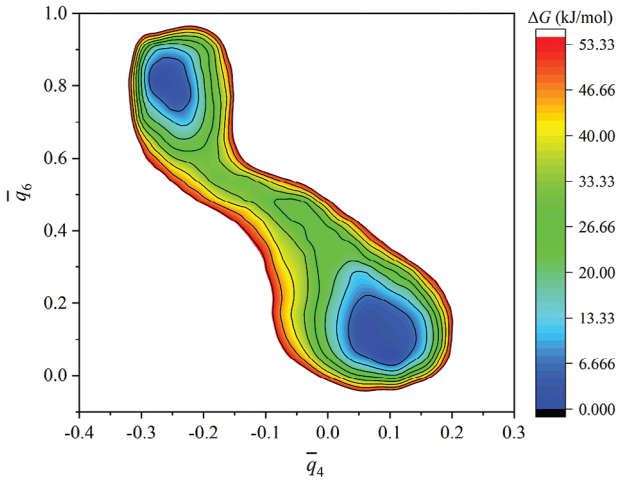

Figure 3. Gibbs free energy contours for nucleation/crystallization of perovskite from a solution of triblock Janus particles at $T = 321$ K and $p = 101.3$ kPa. Free-energy barrier for nucleation at this temperature is (31.8 ± 0.9) kJ (mol Janus particles), i.e., (11.9 ± 0.3) k_BT. Contours are $2.5k_BT$ apart.

strong patch-patch interactions can stabilize the diamond lattice. A further increase of the patch width (getting close to coverage the entire particle surface with patches) stabilizes close packed (fcc or hcp) lattices, not shown here. Hereafter we report simulation results on triblock Janus particles with patch widths 75°, 110°, and 130° for pyrochlore, perovskite, and diamond lattices, respectively. For the patch widths near the boundaries there is a possibility of competition between the two adjacent lattices, however, for the patch widths chosen here, Janus particles self-assemble to the corresponding reported lattices. The respective melting temperatures, obtained from our metadynamics simulations in the ($\bar{q}_6$, $\bar{q}_4$) space, at a pressure $p = 101.3$ kPa are 310, 321, and 285 K. We have shown in **Figure 3**, the free-energy contours for equilibrium between a solution of Janus particles ($\theta = 110°$) and the perovskite lattice, as a typical example.

By gradually imposing the biasing potentials, the system was pushed to perform several round trips between the two basins corresponding to the coexisting phases, to be able to accurately calculate the free energy landscape. Both disordered and crystalline phases are characterized by contours of zero free energy at $\bar{q}_4 \approx \bar{q}_6 \approx 0.1$ and $\bar{q}_4 \approx -0.25$ and $\bar{q}_6 \approx 0.8$, respectively. The disordered phase of triblock Janus particles must surmount a barrier height of 31.8 kJ/(mol Janus particles) to convert to the perovskite lattice. We have no experimental or theoretical report on the barrier height for nucleation of perovskite to compare our calculated value with it. However, experimental[6] and computational[32,40–42] reports on the barrier height for nucleation of a 2D kagome lattice from solution are (5–10) k_BT. Our calculated barrier height (11.9 k_BT) is comparable with the reported values in the literature for a similar process.

4.3. Mechanism of Self-Assembly

Historically, nucleation of a solid phase from liquid is explained in terms of classical nucleation theory. According to this theory, the precursors formed initially as a result of spontaneous fluctuations in the solution, are compact and have the structure of the solid phase. While this theory has practical success in providing quantitative estimates of nucleation rates and free energy barriers, recent experimental and simulation reports on proteins crystallization,[54] crystallization of metallic alloys,[55] and colloid crystallization[56,40–42] found evidence for another picture of nucleation from solution. According to this picture, nucleation from solution follows a two-step process. The first step is a densification into clusters that are still liquid-like. The second step is the rearrangement of the particles in the liquid-like cluster into solid nuclei, which have the same structure as the final crystal. Recently, we have shown that nucleation of a kagome lattice from a solution of triblock Janus particles obeys this two-step mechanism.[40–42]

In order to reveal the 3D mechanism of nucleation of triblock Janus particles, we have done biased sampling simulations. To understand whether formation of disordered aggregates from a dilute solution of Janus particles is a prerequisite for formation of ordered solid nuclei, the cluster size is chosen as one of the order parameters. The number of connected particles within a cutoff distance, the cluster size, N_{cluster}, is defined as:

$$N_{\text{cluster}} = \sum_{i=1}^{N} \frac{1}{N_b(i)} \sum_{j \in N_b(i)} \frac{1}{1 + e^{\alpha(r_{ij} - r_C)}} \tag{8}$$

where r_{ij} is the center-of-mass distance between particles i and j, r_C is the cutoff distance (7.5 nm), and $\alpha = 50\ \text{nm}^{-1}$ is an exponent. The possibility of nucleation and growth of crystalline nuclei from the solution is analysed in terms of the order parameters $\bar{q}_6$ and $\bar{q}_4$, which identify the local crystallinity. Metadynamics simulations in the space of cluster size and $\bar{q}_6$, as the driving coordinates, are done to calculate the free energy surface. In our biased sampling simulations, we add biasing potentials on the coordinates of the connected particles in the largest cluster to increase its size and to generate crystalline nuclei within the largest cluster. The number of crystalline particles inside the largest cluster, N_{crystal}, is calculated based on the local order parameters $\bar{q}_6$ and $\bar{q}_4$. Free energy contours in terms of cluster size and crystal size for nucleation and growth of pyrochlore from the solution are shown in **Figure 4**.

The nucleation proceeds first through the increase in the size of the disordered clusters and a subsequent increase in the local crystallinity. Within the small liquid-like clusters only small crystalline nuclei are formed. Such small nuclei are not stable and melt back to liquid. When the size of liquid-like cluster exceeds a threshold value, nucleation path proceeds through formation and growth of ordered crystalline nuclei in the cluster. Should the nucleation choose the "classical" path, i.e., the emergence of small crystalline embryos and their growth to a critical size, a higher free energy barrier has to be surmounted. By choosing the two-step mechanism of nucleation, the system crosses a lower free energy barrier for crystallization.

Similar metadynamics simulations in the space of cluster size and crystal size ($\bar{q}_6$) are done to investigate the mechanisms of nucleation and growth of perovskite and diamond lattices from the solution of triblock Janus particles. The results, shown in **Figures 5** and **6**, reveal a two-step mechanism of nucleation, as well.

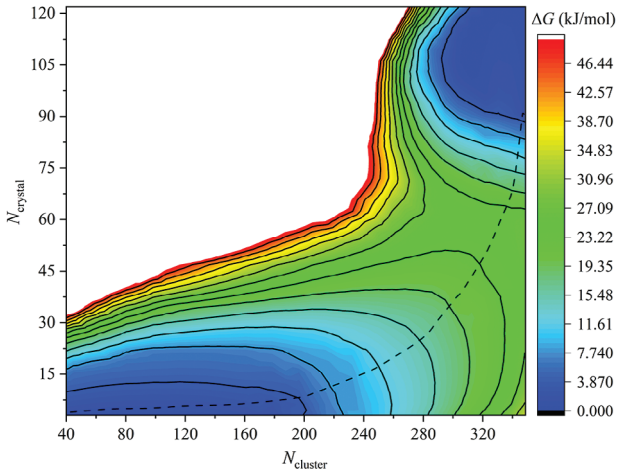

Figure 4. Gibbs free energy contours for nucleation/crystallization of pyrochlore from a solution of triblock Janus particles at $T = 310$ K and $p = 101.3$ kPa. The dashed curve shows the minimum-free-energy path. Free-energy barrier for nucleation at this temperature is (24.6 ± 1.1) kJ/(mol Janus particles), i.e., (9.5 ± 0.4) k_BT. Contours are $1.5k_BT$ apart.

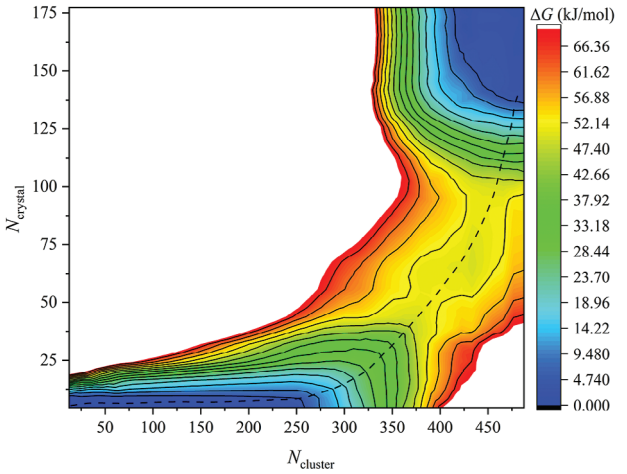

Figure 6. Gibbs free energy contours for nucleation/crystallization of diamond from a solution of triblock Janus particles at $T = 285$ K and $p = 101.3$ kPa. The dashed curve shows the minimum-free-energy path. Free-energy barrier for nucleation at this temperature is (51.5 ± 2.1) kJ/(mol Janus particles), i.e., (21.7 ± 0.9) k_BT. Contours are 2.0 k_BT apart.

The free energy barriers to nucleation for pyrochlore, perovskite, and diamond are 9.5, 11.4, and 21.7 k_BT, respectively. For perovskite the barrier height calculated using cluster size and crystal size as order parameters well agrees with that calculated using $\bar{q}_6$ and $\bar{q}_4$ (Figure 3). In other words, the choice of either set of order parameters does not influence the nucleation/crystallization path and the mechanism of nucleation. This is yet another proof that the stabilities of self-assembled structures and the pathways to nucleation/crystallization are not forced by the bias imposed on the system.

There is no experimental report on the self-assembly of triblock Janus particles to 3D lattices, to compare our calculated barrier heights with. The barrier height for both pyrochlore and perovskite (≈10 k_BT), however, are within the expected range for phase ordering of colloidal particles. Previous experimental[6] and simulation[32,40–42] investigations report a barrier height of (5–10) k_BT for nucleation of the 2D kagome lattice from a solution of triblock Janus particles. The barrier for diamond, however, is much higher than those of pyrochlore and perovskite. One possible reason is that the present triblock Janus particles do not have a correct symmetry for nucleation to diamond. The narrow window of patch width and the large free energy barrier to nucleation of diamond explain why it is difficult experimentally to fabricate diamond-structures from triblock Janus particles as building blocks.

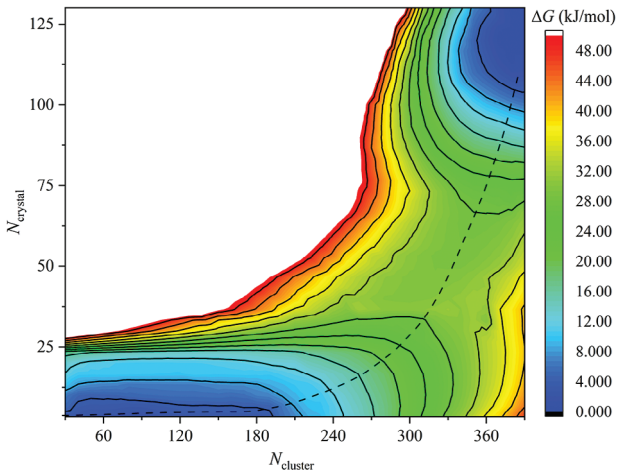

Figure 5. Gibbs free energy contours for nucleation/crystallization of perovskite from a solution of triblock Janus particles at $T = 321$ K and $p = 101.3$ kPa. The dashed curve shows the minimum-free-energy path. Free-energy barrier for nucleation at this temperature is (30.5 ± 1.6) kJ/(mol Janus particles), i.e., (11.4 ± 0.6) k_BT. Contours are $1.5k_BT$ apart.

The Gibbs free energies and the fraction of cluster particles in crystalline surroundings are depicted in **Figure 7** as a function of cluster size, along the respective minimum-free-energy paths for the three crystallization processes. To calculate the minimum-free-energy path, first adaptive-numerical-bias metadynamics[46] is employed to map the rugged free energy landscape in the space of order parameters (Figures 4–6). Then a path-searching algorithm, developed by Fu et al.,[57] is employed to find the minimum free energy path along the order parameters. This method is an iterative procedure to explore the lowest free energy point in the vicinity of the previously calculated free energy points, to connect the chosen free energy basins. Similar to the method by Ensing et al.,[58] it gradually selects the lowest free energy point among all the points on the surface of a circle (in the 2D potential energy surface) centered on a previously found minimum. This point is considered as the starting point for searching for the next minimum.

Figure 7 shows that in the initial stages of nucleation from a solution of Janus particles, $\Delta G = 0$, free energy is needed mainly to increase the cluster size. The free energy cost for formation of small clusters is low, and it is comparable for all three crystallization pathways. The free energy increases almost linearly with the cluster size, as does the fraction of crystal-like particles, which

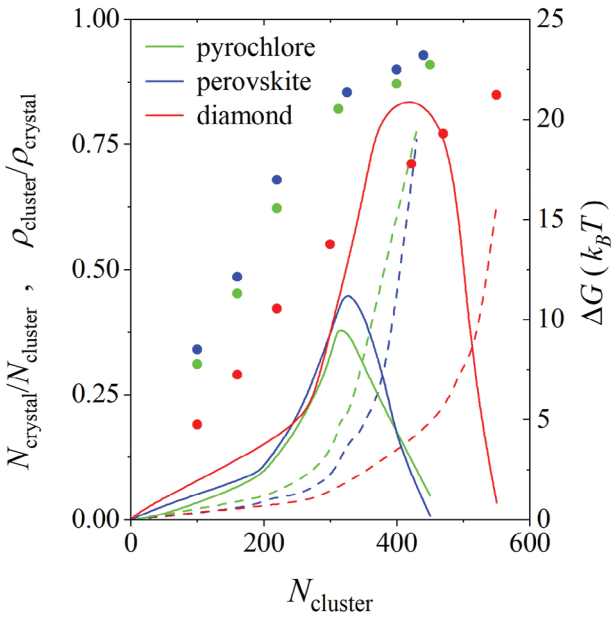

Figure 7. Crystalline fraction of the Janus particles in the dense cluster (dashed curves), the ratio of the density of the cluster to the density of the corresponding crystal (points), and the Gibbs free energy profile (full curves) along the minimum free energy paths, for the formation of crystal nuclei (pyrochlore: green; perovskite: blue; diamond: red).

however stays low. In this regime the nucleation path mainly involves travelling along one of the reaction coordinates, i.e., densification. At some threshold size (200–230 particles) the free energy begins to increase super-linearly before going through a maximum (free energy barrier). This threshold size (200–230 particles) weakly depends on the crystal structure, because over this regime only amorphous liquid-like clusters form and grow. In other words, a similar densification process precedes formation of the three crystals. At a higher cluster size (approximately above 250, 270, and 350 for pyrochlore, perovskite and diamond, respectively) the crystalline fraction increases rapidly. This is due to the dense, but liquid-like particles reorienting into crystalline configurations, starting from the surface of the crystalline nucleus. In this second regime, the nucleation proceeds along the second reaction coordinates, crystallization. Therefore, the second threshold as well as the size of the critical nucleus (corresponding to the top of barrier height in Figure 7, i.e., 315, 335, 415 for pyrochlore, perovskite, and diamond, respectively) depend on the crystal structure. In phase 1 (densification) a lower free energy increase is found for Janus particles with wider patches, i.e., those which are going to crystallize to diamond compared to perovskite and pyrochlore. This can be interpreted in terms of stronger patch-patch interactions in wider patch particles. This order is reversed in phase 2, the crystallization within the dense cluster: a much larger free energy barrier is observed for the formation of diamond than of perovskite and pyrochlore. In other words, proper orientation of triblock Janus particles to tetrahedral subunits, assembling to diamond, involves surmounting a large free energy barrier. A speculative explanation is that the wider patches allow the particles many energetically degenerate orientations in the disordered dense cluster; and when they snap into the relatively rigid tetrahedral diamond conformations they pay an entropic penalty. This is in line with the report by Zanjani et al.[59] on the challenge in the self-assembly of cubic clusters to open cubic lattices, due to the existence of energetically degenerate states.

We provide snapshots of the simulations in **Figures 8–10**, to better elucidate structure formation along the nucleation path. The snapshots are shown for the largest cluster in the simulation, starting from the time the cluster is large enough to allow formation of small crystalline nuclei. For pyrochlore, **Figure 8a** shows inside the liquid cluster a small nucleus, whose members are arranged like in the final crystal. There are other crystalline nuclei in the liquid cluster, but we only show the largest one. The liquid cluster consists of tetrahedrally ordered smaller structures (zoomed-in part in Figure 8a), joined into rings. The tetrahedral arrangement of Janus particles is more evident at the boarder between the liquid cluster and the solution. The rings have a variety of sizes (Figure 8b), but those which eventually nucleate to pyrochlore are the six-membered rings, i.e., consistent with the symmetry of the lattice. With the passage of time and further driving the simulations toward lattice formation through biased-sampling simulations, the liquid cluster attracts more particles and becomes more compact at the same time. We show the ratio of the density of the cluster to the density of the crystal in Figure 7. The volumes of the cluster and the crystal are defined as the volumes of spheres with the same radii as the radii of gyration of the cluster and a well grown postcritical crystal inside the cluster, respectively. The cluster becomes more compact with increasing its size. The increase in the density is, however, more pronounced for smaller clusters, which host only small size crystals. Following this regime, the clusters still become more compact, but to a lesser extent. The clusters which are going to crystallize to diamond are less compact than those preceding pyrochlore and perovskite.

With the growth and compactness of the liquid cluster, the crystalline regions grow inside it. When a crystalline nucleus is large enough to survive, the liquid-like particles at its boarder with the liquid cluster reorient to adopt the symmetry of the crystal. Upon formation of a nucleus of the critical size (Figure 8c), the rest of the liquid quickly converts to the solid phase. The structure of a well grown pyrochlore crystallite, surrounded by liquid-like particles is shown in Figure 8d.

We have provided similar series of snapshots for the nucleation/crystallization of perovskite and diamond lattices in Figures 9 and 10, respectively. Self-assembly of perovskite (**Figure 9**) involves formation of tetrahedral structures, some of which are visible at the boarder of cluster with the liquid solution, which subsequently attach together and rearrange to trigonal- and inverted-bipyramids and subsequently to octahedral structures (Figure 9a). In the self-assembly of the diamond structure (Figure 9), due to the stronger patch-patch attractions by wider patches, a amorphous network of connected particles is formed in the early stages of assembly (**Figure 10a**). The Janus particles in this network are tetrahedrally as well as linearly connected. As self-assembly progresses, linear segments disappear in favor of a larger and more compact network of tetrahedral structures (Figure 10b,c). Proper orientations of tetrahedral subunits to diamond, however, requires overcoming a larger free energy barrier than for pyrochlore and perovskite. A

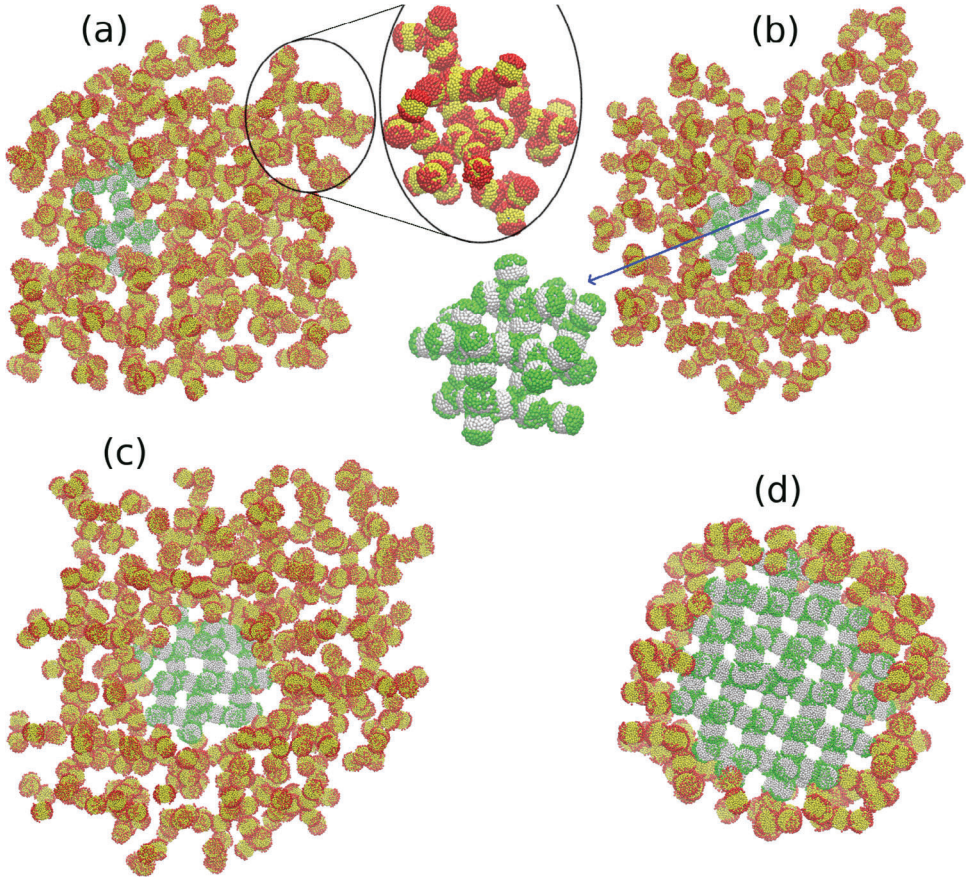

Figure 8. Simulation snapshots of the largest cluster for the nucleation/crystallization of pyrochlore from a solution of triblock Janus particles in water at $T = 310$ K and $p = 101.3$ kPa. For clarity, the surface charges and the solvent particles are not shown. The zoomed-in parts in snapshots (a) and (b) show tetrahedrally ordered structures in the liquid cluster and the structure of a crystalline nucleus, surrounded by the disordered cluster, respectively. Snapshots (a-d) belong to simulation times 1.8, 2.2, 3.2, and 3.8 μs, respectively.

reason for this might be found by comparing the final snapshots (Figures 8d, 9d, and 10d). The crystallites of pyrochlore and perovskite are embedded in orientationally disordered, but compact amorphous clusters (Figures 8d and 9d). They can grow by adjacent particles rotating into position. In contrast, the amorphous cluster surrounding the diamond crystallite (Figure 109d) appears much loser and still containing more non-tetrahedral units. This can be further confirmed by the results on the density of the clusters in Figure 7; clusters which are going to crystallize to diamond are less compact than those of pyrochlore and perovskite. In the amorphous cluster surrounding the small diamond nuclei, adjacent molecules must compact *and* reorient to join the crystallite. This is in line with the entropy argument used above. We may summarize by noting that similar two-step mechanisms are operational in the nucleation of crystals for all three lattice structures, but the details are slightly different.

4.4. Sequence of Self-Assembly

We investigate the pathway from liquid solution to pyrochlore lattice, as a typical example, by analyzing the evolution of order in the system. To this end, we track the concentrations of Janus particles being part of different structures. Starting from a solution of randomly distributed Janus particles in water, in which the Janus particles have no contacts together (**Figure 11**), during the course of *NpT*-ensemble simulations, Janus particles stick together via the patches (≈0.01 μs). The particles further attach together to form dimers, trimers, and longer chains, with the chain population paeking at ≈0.1 μs. The short chains are stretched due to the repulsion between their equatorial regions and maximum overlap between attractive patches. Therefore, the chain grows by adding new particles to its ends. This mechanism of one-by-one addition of particles to the chain ends is in agreement with confocal fluorescence microscopy experiments[60] and with our recent simulation reports.[28,40–42] Entropy, however, disfavors stretched chains. Therefore, further addition of Janus particles to chains causes them to bend and introduces triangular and tetrahedral branch points. This leads to the formation of a 3D percolating network of Janus particles. In other words, in agreement with experiment,[6] the chains are intermediate low-density aggregates, which form in the early stages of assembly; initially their concentration increases and subsequently decreases. The particles in the percolating network, which still have a liquid-like structure, generate further branches and bond

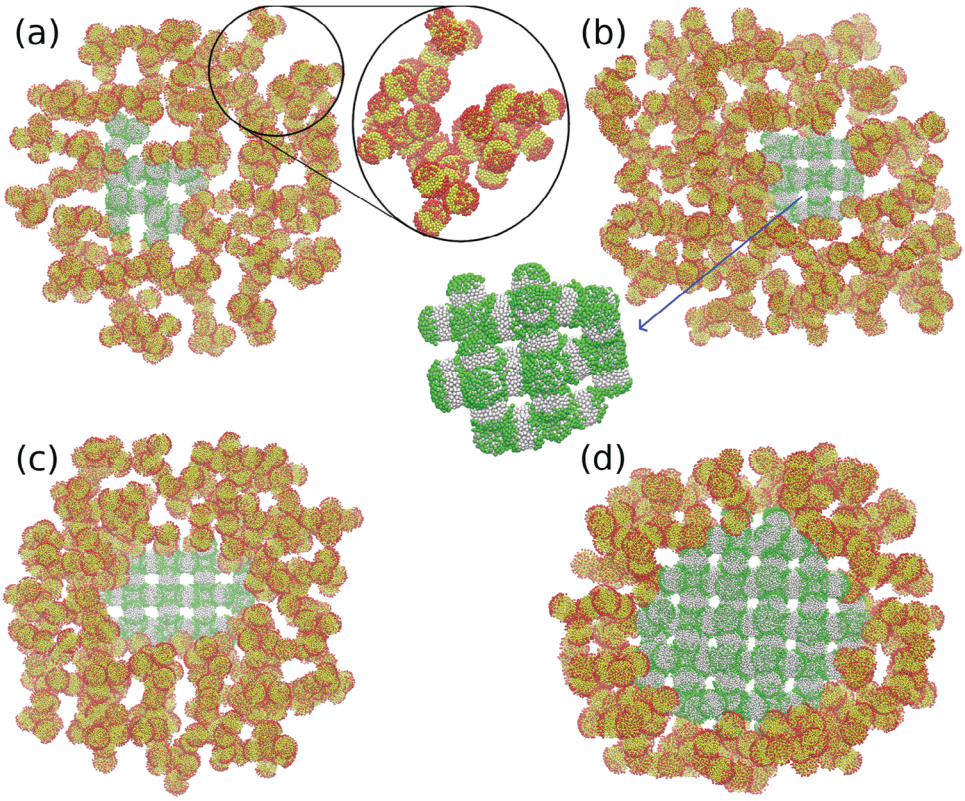

Figure 9. Snapshots of simulation box for nucleation/crystallization of perovskite from a solution of triblock Janus particles in water at $T = 321$ K and $p = 101.3$ kPa. For clarity, the surface charges and the solvent particles are not shown. The zoomed-in part in snapshot (a) shows tetrahedral, trigonal bipyramid, inverted bipyramid, and octahedral structures in the liquid cluster. In snapshot (b) the structure of a crystalline nucleus, surrounded by the disordered cluster, is zoomed in. Snapshots (a-d) belong to simulation times 1.7, 2.8, 3.1, and 4.2 μs, respectively.

to neighbouring particles in a tetrahedral geometry and eventually generate ring structures. Such tetrahedral and ring structures have been observed in fluorescence microscopy experiments of Chen et al.[2] on the staged-assembly of triblock Janus particles to there-dimensional metastructures. The initial rings have different sizes, but with the passage of time and pushing the nucleation pathway toward formation of pyrochlore, the five- to eight-membered rings become dominant (≈2 μs). The six-membered rings are most stable and, with time, the other rings rearrange to become six-membered rings, which have the same symmetry as the pyrochlore lattice. The pyrochlore lattice nucleates when a threshold fraction of particles with tetrahedral environment (>0.3) has been formed. This agrees with former simulation reports in the literature, where the pyrochlore lattice is self-assembled from tetrahedral clusters as building blocks.[23,27,35] Our study, however, differ from those in that we use triblock Janus particles as the building blocks. The triblock Janus particles form tetrahedral structures as intermediate structures, which subsequently convert to the pyrochlore lattice. The regime of slow increase in the fraction of particles belonging to the pyrochlore lattice (1 μs < t <3.2 μs) in Figure 11 shows the nucleation step and the regime of fast increase (t > 3.2 μs) represents the growth step. It is worth mentioning that experimentally self-assembled 3D structures from triblock Janus particles are limited to 3D tetrahedral and octahedral clusters, but no 3D open structure is fabricated. Therefore, lack of experimental reports on the self-assembly of 3D colloidal lattices forbids us to compare our findings on the mechanism of phase ordering process and the calculated barrier heights with experiment. However, the growth dynamics of tetrahedral and octahedral clusters to a higher order assembly of clusters in three dimensions through formation of chains, pores, and networks is consistent with the fluorescence microscopy experiments of Chen et al.[2]

Consistent with experiment[2,6] and analytical theory,[61] entropy plays a fundamental role in stabilization of self-assembled open lattices in this work. The rotational and vibrational entropies of Janus particles lower the free energy of open lattices; therefore, the temperature and the patch width influence the stabilities of the phases, hence, the barrier heights to crystallization. However, previous reports on the nucleation of colloidal particles[62] and the phase behavior of a detailed model of triblock Janus particles in two dimensions[28,40–42] show that the concentration of particles, temperature, and patch width affect the barrier heights and the types of phases involved, but not the mechanism of nucleation. Therefore, we speculate that the two-step mechanism of nucleation discussed here not to depend on the concentration of Janus particles, the temperature, and the patch width. The barrier heights and the types of phases, however, depend on such factors.

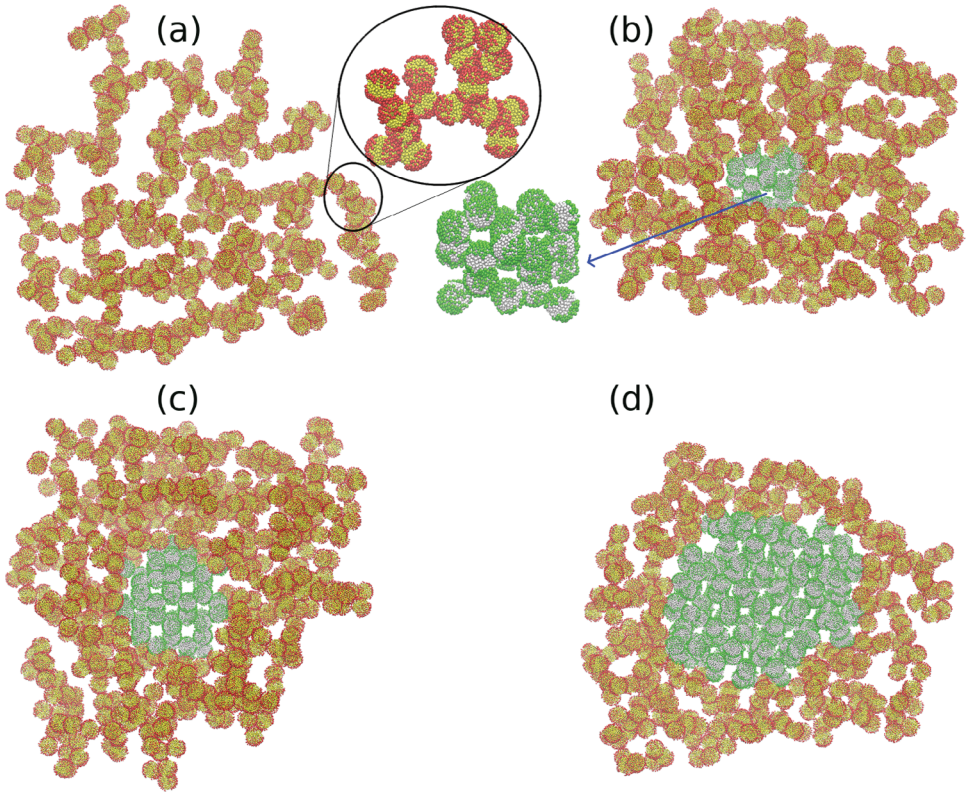

Figure 10. Snapshots of simulation box for nucleation/crystallization of diamond from a solution of triblock Janus particles in water at $T = 285$ K and $p = 101.3$ kPa. For clarity, the surface charges and the solvent particles are not shown. The zoomed-in parts in snapshots (a) and (b) show tetrahedrally connected Janus particles in the liquid cluster and the structure of a diamond nucleus, surrounded by the liquid cluster, respectively. Snapshots (a–d) belong to simulation times 1.1, 2.6, 4.7, and 5.3 µs, respectively.

5. Conclusions

We simulate the self-assembly of triblock Janus particles (attractive patches at the poles and repulsive charges near the equator) from a fluid into different 3D open lattices, namely, pyrochlore, perovskite, and diamond. The objectives are both the relative stability of the crystalline modifications depending on the particle architecture and the dynamics mechanism of the assembly processes. The stability of each of the three crystal structures at ambient temperatures and pressures depends on the width of the hydrophobic patches at the poles of the Janus particles. Particles with narrow patches (opening angle $56° < \theta < 87°$), which allow three bonds per patch to stabilize tetrahedral subunits, self-assemble to a pyrochlore lattice. Intermediate patches ($87° < \theta < 122°$) allow for four contacts per patch to form octahedral units and stabilize the denser perovskite lattice. Only very wide patches ($125° < \theta < 135°$) provide strong enough patch-patch interactions to stabilize a diamond lattice.

The mechanism of nucleation of the three open lattices from the solution of triblock Janus particles in water proceeds in steps. Isolated Janus particles attach with one another via the sticky patches and form dimers, trimers, and short chains. This step-by-step chain growth has also been found in experiments.[60] Eventually, the chains bend and form triangular and subsequently tetrahedral branch points. This leads to a 3D percolating network of Janus particles containing five- to eight-membered rings. Eventually, the ring sizes that match the symmetry of the lattice becomes dominant (six-membered rings for pyrochlore and diamond and six- and eight-membered rings for perovskite). The pyrochlore and diamond lattices nucleate when a threshold fraction of particles with tetrahedral environment has been formed in the system. This agrees with former simulation reports in the literature, where the pyrochlore lattice self-assembles from tetrahedral building blocks.[23,27,35]

A main finding of this study is that a dense, but amorphous and disordered cluster has to be formed first. Only then, can crystalline nuclei emerge inside it. This two-step mechanism has been observed for the nucleation for all three lattices: In the first step, Janus particles densify via their hydrophobic patches into a disordered, amorphous cluster. In he second step, they reorient almost in place to form crystalline nuclei. While the particles in the liquid cluster do form, depending on their patch sizes, tetrahedral and/or octahedral units do not turn into their crystal-compatible orientations until the liquid cluster has grown to a threshold size, approximately 250, 270, and 350 for pyrochlore, perovskite and diamond, respectively. During the first densification process, only small crystalline nuclei may form and some of them melt back to liquid. In the second step (crystallization) the size of the cluster does not increase noticeably, rather, its orientational ordering starts from the cluster boarder. In this step a critical crystalline nucleus is formed, which subsequently grows much faster.

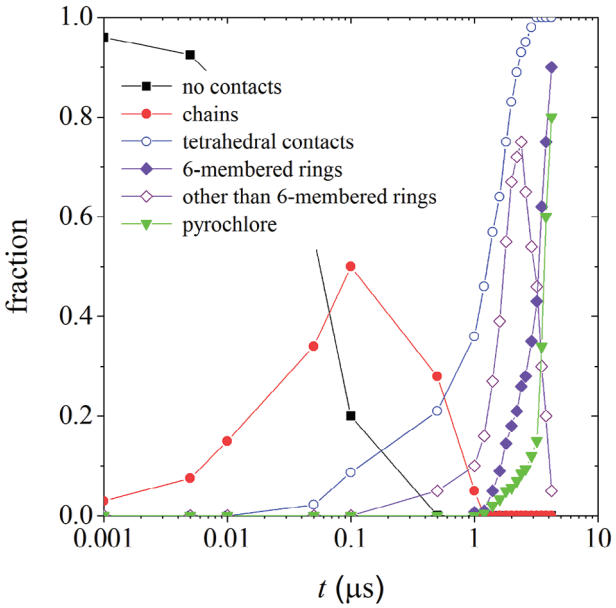

Figure 11. Time-dependence of the structural evolution of triblock Janus particles, in the self-assembly of pyrochlore from a solution, expressed as fraction of particles being part of the respective structure: isolated Janus particles, particles in chains, particles having tetrahedral contacts, particles involved in rings (6-membered rings and other than 6-membered rings), and particles in a pyrochlore lattice.

Free energy barriers for nucleation of pyrochlore and perovskite, 9.5 and 11.4 k_BT, respectively, are close to the reported values for the nucleation of the 2D kagome lattice on a substrate from a solution of triblock Janus particles, (5–10) k_BT.[6,32,40–42] However, the barrier height for nucleation of diamond is much larger (21.7 k_BT). This outlier position may possibly be understood by entropic arguments: in the disordered state the wide hydrophobic patches allow a larger number of energetically equivalent arrangements. These, in turn lead to the disordered, loose agglomerates being more stable. As a result, an entropic barrier must be overcome when particles turn into their crystal orientations, *and* the amorphous cluster still has to further compact before crystallization can proceed.

To summarize, the choice of the detailed model of Janus particles allowed us to expand the existing literature on the self-assembly of triblock Janus particles in three aspects. First, we allowed an assembly process, in which individual triblock Janus particles (and not preformed structures with the proper symmetry of the target lattices) are the building blocks. Second, by performing biased sampling simulations, we investigate the mechanism of self-assembly. We have calculated the free-energy barriers to nucleation of the pyrochlore, perovskite, and diamond lattices, which can provide experimentalists with an estimate of the ease of fabrication of these lattices. Third, we have provided mechanistic aspects of the self-assembly process, elucidating the structural evolution of Janus particle aggregates. Interestingly, we found intermediate structures, which are reported in experiment[2] and are used in some recent studies[23,27,35] as building blocks for self-assembly of the corresponding lattices.

Acknowledgements

This work has been supported by the Deutsche Forschung gemeinschaft via the SFB-TRR 146 "Multiscale Simulation Methods for Soft Matter Systems", Project B8.

Conflict of Interest

The authors declare no conflict of interest.

Data Availability Statement

The data that support the findings of this study are available from the corresponding author upon reasonable request.

Keywords

colloid crystallization, Janus particles, nucleation, open lattices, self-assembly

Received: July 26, 2023
Revised: October 20, 2023
Published online: November 22, 2023

[1] S. Jiang, Q. Chen, M. Tripathy, E. Luijten, K. S. Schweizer, S. Granick, *Adv. Mater.* **2010**, *22*, 1060.
[2] Q. Chen, S. C. Bae, S. Granick, *J. Am. Chem. Soc.* **2012**, *134*, 11080.
[3] Y. Cui, J. Wang, J. Liang, H. Qiu, *Small* **2023**, *19*, 2207609.
[4] F. Naderi Mehr, D. Grigoriev, R. Heaton, J. Baptiste, A. J. Stace, N. Puretskiy, E. Besley, A. Böker, *Small* **2020**, *16*, 2000442.
[5] S. K. Ghosh, A. Böker, *Macromol. Chem. Phys.* **2019**, *220*, 1900196.
[6] Q. Chen, S. C. Bae, S. Granick, *Nature* **2011**, *469*, 381.
[7] Y. Geng, S. Ling, J. Huang, J. Xu, *Small* **2020**, *16*, 1906357.
[8] C. Li, M. Zhao, X. Zhou, H. Li, Y. Wang, X. Hu, M. Li, L. Shi, Y. Song, *Adv. Opt. Mater.* **2018**, *6*, 1800651.
[9] S. Li, J. He, S. Qiao, X. Zhang, B. Liu, *Small* **2023**, *19*, 2300642.
[10] D. Luo, C. Yan, T. Wang, *Small* **2015**,*11*, 5984.
[11] S.-W. Chung, D. S. Ginger, M. W. Morales, Z. Zhang, V. Chandrasekhar, M. A. Ratner, C. A. Mirkin, *Small* **2005**, *1*, 64.
[12] W. Zhou, Q.-Y. Lin, J. A. Mason, V. P. Dravid, C. A. Mirkin, *Small* **2018**, *14*, 1802742.
[13] A. M. Wong, K. Je, C. Y. Zheng, L. Jibril, Z. Miao, S. C. Glotzer, C. A. Mirkin, *Nano Lett.* **2023**, *23*, 116.
[14] M. He, J. P. Gales, É. Ducrot, Z. Gong, G.-R. Yi, S. Sacanna, D. J. Pine, *Nature* **2020**, *585*, 524.
[15] M. Vafaeezadeh, W. R. Thiel, *Angew. Chem., Int. Ed.* **2022**, *61*, e202206403.
[16] F. Sciortino, A. Giacometti, G. Pastore, *Phys. Rev. Lett.* **2009**, *103*, 237801.
[17] E. Bianchi, C. N. Likos, G. Kahl, *Nano Lett.* **2014**, *14*, 3412.
[18] N. A. Mahynski, L. Rovigatti, C. N. Likos, A. Z. Panagiotopoulos, *ACS Nano* **2016**, *10*, 5459.
[19] N. A. García, N. Gnan, E. Zaccarelli, *Soft Matter* **2017**, *13*, 6051.
[20] N. Kern, D. Frenkel, *J. Chem. Phys.* **2003**, *118*, 9882.
[21] N. A. Mahynski, H. Zerze, H. W. Hatch, V. K. Shen, J. Mittal, *Soft Matter* **2017**, *13*, 5397.
[22] W. F. Reinhart, A. Z. Panagiotopoulos, *J. Chem. Phys.* **2018**, *148*, 124506.
[23] D. F. Tracey, E. G. Noya, J. P. K. Doye, *J. Chem. Phys.* **2019**, *151*, 224506.
[24] E. G. Noya, I. Zubieta, D. J. Pine, F. Sciortino, *J. Chem. Phys.* **2019**, *151*, 094502.

[25] T. Dasgupta, G. M. Coli, M. Dijkstra, *ACS Nano* **2020**, *14*, 3957.
[26] I. Q. Matos, F. A. Escobedo, *J. Phys. Chem. B* **2023**, *127*, 3746.
[27] Z.-W. Li, Y.-W. Sun, Y.-H. Wang, Y.-L. Zhu, Z.-Y. Lu, Z.-Y. Sun, *J. Phys. Chem. Lett.* **2021**, *12*, 7159.
[28] K. Bahri, H. Eslami, F. Müller-Plathe, *J. Chem. Theory Comput.* **2022**, *18*, 1870.
[29] Zhang, A. S. Keys, T. Chen, S. C. Glotzer, *Langmuir* **2005**, *21*, 11547.
[30] F. Romano, E. Sanz, F. Sciortino, *J. Chem. Phys.* **2010**, *132*, 184501.
[31] E. G. Noya, C. Vega, J. P. K. Doye, A. A. Louis, *J. Chem. Phys.* **2010**, *132*, 234511.
[32] F. Romano, F. Sciortino, *Nat. Commun.* **2012**, *3*, 975.
[33] W. F. Reinhart, A. Z. Panagiotopoulos, *J. Chem. Phys.* **2016**, *145*, 094505.
[34] D. Morphew, J. Shaw, C. Avins, D. Chakrabarti, *ACS Nano* **2018**, *12*, 2355.
[35] S. Paul, H. Vashisth, *Soft Matter* **2020**, *16*, 1142.
[36] B. Abhishek, A. B. Rao, J. Shaw, A. Neophytou, D. Morphew, F. Sciortino, R. L. Johnston, D. Chakrabarti, *ACS Nano* **2020**, *14*, 5348.
[37] A. Neophytou, V. N. Manoharan, D. Chakrabarti, *ACS Nano* **2021**, *15*, 2668.
[38] L. Y. Rivera-Rivera, T. C. Moore, S. C. Glotzer, *Soft Matter* **2023**, *19*, 2726.
[39] P. Español, P. Warren, *Europhys. Lett.* **1995**, *30*, 191.
[40] H. Eslami, K. Bahri, F. Müller-Plathe, *J. Phys. Chem. C* **2018**, *122*, 9235.
[41] H. Eslami, N. Khanjari, F. Müller-Plathe, *J. Chem. Theory Comput.* **2019**, *15*, 1345.
[42] H. Eslami, A. Gharibi, F. Müller-Plathe, *J. Chem. Theory Comput.* **2021**, *17*, 1742.
[43] I. P. Madden, L. Wang, J. Simmchen, E. Luijten, *Small* **2022**, *18*, 2107023.
[44] H. Eslami, N. Khanjari, F. Müller-Plathe, *J. Chem. Theory Comput.* **2017**, *13*, 1307.
[45] A. Barducci, M. Bonomi, M. Parrinello, *WIREs Comput. Mol. Sci.* **2011**, *1*, 826.
[46] N. Khanjari, H. Eslami, F. Müller-Plathe, *J. Comput. Chem.* **2017**, *38*, 2721.
[47] P. J. Steinhardt, D. R. Nelson, M. Ronchetti, *Phys. Rev. B* **1983**, *28*, 784.
[48] J. S. Van Duijneveldt, D. Frenkel, *J. Chem. Phys.* **1992**, *96*, 4655.
[49] H. Eslami, P. Sedaghat, F. Müller-Plathe, *Phys. Chem. Chem. Phys.* **2018**, *20*, 27059.
[50] P. B. Warren, *Phys. Rev. E* **2003**, *68*, 066702.
[51] H.-J. Qian, P. Carbone, X. Chen, H. A. Karimi-Varzaneh, C. C. Liew, F. Müller-Plathe, *Macromolecules* **2008**, *41*, 9919.
[52] F. Müller-Plathe, *Comput. Phys. Commun.* **1993**, *78*, 77.
[53] H. Eslami, M. Khani, F. Müller-Plathe, *J. Chem. Theory Comput.* **2019**, *15*, 4197.
[54] P. R. Ten Wolde, D. Frenkel, *Science* **1997**, *277*, 1975.
[55] S. Moniri, H. Bale, T. Volkenandt, Y. Wang, J. Gao, T. Lu, K. Sun, R. O. Ritchie, A. J. Shahani, *Small* **2020**, *16*, 1906146.
[56] D. Gebauer, J. D. Gale, H. Cölfen, *Small* **2022**, *18*, 2107735.
[57] H. Fu, H. Chen, X. '. Wang, H. Chai, X. Shao, W. Cai, C. Chipot, *J. Chem. Inf. Model.* **2020**, *60*, 5366.
[58] B. Ensing, A. Laio, M. Parrinello, M. L. Klein, *J. Phys. Chem. B* **2005**, *109*, 6676.
[59] M. B. Zanjani, I. C. Jenkins, J. C. Crocker, T. Sinno, *ACS Nano* **2016**, *10*, 11280.
[60] Y. Wang, Y. Wang, D. R. Breed, V. N. Manoharan, L. Feng, A. D. Hollingsworth, M. Weck, D. J. Pine, *Nature* **2012**, *491*, 51.
[61] X. Mao, Q. Chen, S. Granick, *Nat. Mater.* **2013**, *12*, 217.
[62] S. Auer, D. Frenkel, *Nature* **2001**, *409*, 1020.

